Capturing Enzyme Structure Prior to Reaction Initiation: Tropinone Reductase-II−Substrate Complexes‡

Atsuko Yamashita,[§,||] Masaharu Endo,[||] Tsuneyuki Higashi,[⊥] Toru Nakatsu,[¶,||] Yasuyuki Yamada,[@] Jun'ichi Oda,[||,#] and Hiroaki Kato*[,¶,||]

Structural Biochemistry Laboratory and Membrane Dynamics Research Group, RIKEN Harima Institute at SPring-8, 1-1-1 Kouto, Mikazuki, Sayo, Hyogo 679-5148, Japan, Institute for Chemical Research, Kyoto University, Uji, Kyoto 611-0011, Japan, Rigaku Corporation, 3-9-12 Matsubara, Akishima, Tokyo 196-8666, Japan, Graduate School of Biological Sciences, Nara Institute of Science and Technology, Takayama, Ikoma, Nara 630-0101, Japan, and Fukui Prefectural University, 4-1-1 Kenjyojima, Matsuoka, Fukui 910-1195, Japan

Received December 2, 2002; Revised Manuscript Received March 10, 2003

ABSTRACT: To understand the catalytic mechanism of an enzyme, it is crucial to determine the crystallographic structures corresponding to the individual reaction steps. Here, we report two crystal structures of enzyme−substrate complexes prior to reaction initiation: tropinone reductase-II (TR-II)−NADPH and TR-II−NADPH−tropinone complexes, determined from the identical crystals. A combination of two kinetic crystallographic techniques, a continuous flow of the substrates and Laue diffraction measurements, enabled us to capture the transit structures prior to the reaction proceeding. A structure comparison of the enzyme−substrate complex elucidated in this study with the enzyme−product complex in our previous study indicates that one of the substrates, tropinone, is rotated relative to the product so as to make the spatial organization in the active site favorable for the reaction to proceed. Side chains of the residues in the active site also alter their conformations to keep the complementarity of the space for the substrate or the product and to assist the rotational movement.

An enzyme structure determined by X-ray crystallography is both temporally and spatially averaged. Since most enzymatic reactions are completed in less than a second, which is much shorter than the period of time required for data collection, the visualization of discrete steps in an enzyme-catalyzed reaction is highly unlikely under normal conditions (*1*). Indeed, most published structures of enzyme−substrate complexes are nonproductive complexes, with substrate analogues or inhibitors, or with mutant enzymes. To understand the detailed catalytic mechanism, we should obtain the structure of the productive enzyme−substrate complex, the so-called true Michaelis complex.

Tropinone reductase-II (TR-II; EC 1.1.1.236)[1] catalyzes the NADPH-dependent reduction of a carbonyl group of tropinone to a β-hydroxyl group and produces pseudotropine (ψ-tropine; Scheme 1). TR-II is a 260-residue homodimeric enzyme mainly found in the biosynthetic pathways of tropane alkaloids in some medicinal plants (*2, 3*). The deduced sequence of TR-II indicates that this enzyme is a member of the short-chain dehydrogenase/reductase family (*3*). The first crystallographic structure of TR-II was reported together with the structure of tropinone reductase-I, a homologous protein that also reduces tropinone but exhibits a different reaction stereospecificity (*4*).

Scheme 1

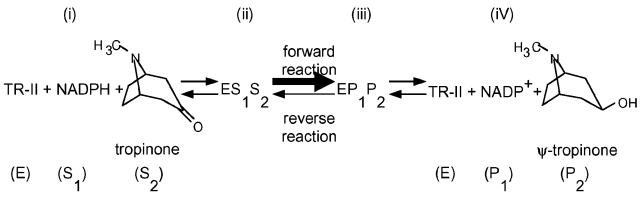

In the process of the TR-II catalytic reaction, four states of the enzyme can be identified as described below since an enzymatic NADP(H) oxidoreduction is described as a one step reaction with an ordered mechanism: (i) E, the free enzyme; (ii) ES_1S_2, the enzyme with the substrates [NADPH (S_1) and tropinone (S_2)] prior to reaction initiation; (iii) EP_1P_2, the enzyme with the products [$NADP^+$ (P_1) and ψ-tropine (P_2)] just after the reaction is completed; and (iv) the free enzyme again after releasing the products (Scheme 1). The crystallographic structures of TR-II determined thus far were either in an unliganded form (*4*) or complexed with $NADP^+$ and ψ-tropine (*5*). The former would be regarded as the free

‡ The atomic coordinates and the structure factors have been deposited in the Protein Data Bank, www.rcsb.org [PDB codes 1ipe (TR-II−NADPH complex) and 1ipf (TR-II−NADPH−tropinone complex)].

* Corresponding author. Phone: +81-791-58-1825. Fax: +81-791-58-1826. E-mail: katohiro@spring8.or.jp.

§ Structural Biochemistry Laboratory, RIKEN.

|| Kyoto University.

⊥ Rigaku Corporation.

¶ Membrane Dynamics Research Group, RIKEN.

@ Nara Institute of Science and Technology.

Fukui Prefectural University.

[1] Abbreviations: TR-II, tropinone reductase-II; ψ-tropine, pseudotropine; E, the free enzyme state of tropinone reductase-II; S_1, NADPH; S_2, tropinone; P_1, $NADP^+$; P_2, pseudotropine; ES_1S_2, tropinone reductase-II−NADPH−tropinone complex (the enzyme−substrate complex state); EP_1P_2, tropinone reductase-II−$NADP^+$−pseudotropine complex (the enzyme−product complex state); ES_1, tropinone reductase-II−NADPH complex.

10.1021/bi0272712 CCC: $25.00
Published on Web 04/19/2003

Table 1: Laue X-ray Diffraction Data and Refinement Statistics

	Data Statistics			
	first data (TR-II−NADPH)		second data (TR-II−NADPH−tropinone)	
solution condition	4 mM NADPH		4 mM NADPH 110 mM tropinone	
space group	$P6_122$		$P6_122$	
cell dimensions	$a = b = 88.6$ Å $c = 338.9$ Å		$a = b = 88.6$ Å $c = 337.2$ Å	
images (*n*)	7		7	
reflections				
observed (*n*)	149 781		155 667	
unique (*n*)	24 496		24 567	
redundancy[a] (*n*)	6.11		6.34	
completeness and *R*-merge[b] (%)	compl.	*R*-merge	compl.	*R*-merge
∞−5.39 Å	81.5	7.9	81.8	8.8
5.39−4.28 Å	87.4	8.4	87.9	9.1
4.28−3.73 Å	86.8	10.7	87.2	10.4
3.73−3.39 Å	86.6	12.7	86.6	11.8
3.39−3.15 Å	86.7	16.8	86.9	15.2
3.15−2.96 Å	87.5	19.9	87.5	18.6
2.96−2.82 Å	86.2	22.4	87.5	21.9
2.82−2.69 Å	87.2	24.1	88.9	23.7
2.69−2.59 Å	86.5	26.3	87.2	26.3
2.59−2.50 Å	82.8	28.0	84.3	27.0
cumulative	85.9	13.4	86.5	13.4
	Refinement Statistics			
resolution (Å)	10−2.5 Å			
10−2.5 Å				
R-factor[c]/R_{free}	0.195/0.268		0.197/0.265	
rms deviations				
bond length (Å)	0.007		0.008	
bond angles (deg)	1.302		1.332	
dihedral angles (deg)	24.569		23.812	
improper angles (deg)	0.669		0.685	

[a] Redundancy = number of observations/number of unique reflections. [b] *R*-merge = $\sum||F|^2 - <|F|^2>|/\sum|F|^2$, calculated for singlet reflections. [c] *R*-factor = $\sum||F_o| - |F_c||/\sum|F_o|$ (5% randomly omitted reflections were used for R_{free}).

enzyme E state, and the latter as the enzyme−product complex EP_1P_2 state. To elucidate the catalytic mechanism of TR-II in detail, it is crucially important to know the structure of enzyme−substrate Michaelis complex, the ES_1S_2 state. Here, we present the structure of the TR-II−NADPH−tropinone complex, the ES_1S_2 state Michaelis complex, together with the TR-II−NADPH complex structure at 2.5 Å resolution. To capture the structure of the Michaelis complex, we applied a multiwavelength Laue X-ray diffraction method with a crystal saturated by a large excess of substrate.

EXPERIMENTAL PROCEDURES

Laue Data Collection with Flow-Cell Experiment. TR-II from *Datura stramonium* was expressed and purified as described previously (*6*). The crystals of TR-II complexed with NADPH were obtained by cocrystallization in the presence of 4 mM NADPH using lithium sulfate as a precipitant (*5*). Laue diffraction data were collected at BL-18B station, Photon Factory, at room temperature (15 °C) by the use of Weissenberg/Laue camera for macromolecular crystals with 430 mm crystal-to-detector distance and Fuji 40 × 80 cm imaging-plates. The TR-II crystal for data collection was mounted in a flow cell (0.7 mm in diameter) (*7*). In the first place, a solution containing 4 mM NADPH, 0.1 M HEPES-Na, pH 7.5, 2.0 M Li_2SO_4, and 1 mM DTT was passed across the crystal at a rate of 0.1 mL min^{-1} to ensure NADPH binding. The first data collection series (for TR-II−NADPH complex) was started 15 min after initiating the flow at room temperature. Then the same crystal was irrigated with the same solution containing an additional 110 mM tropinone at a flow rate of 1.0 mL min^{-1}. After 15 min of irrigation, the second data series (for TR-II−NADPH−tropinone complex) was collected. For each series of experiments, seven polychromatic X-ray exposures (30 ms each) were recorded at different spindle axis positions, and all exposures were carried out within 15 min. Under the experimental conditions, the kinetic constants of TR-II as apparent K_m for NADPH, for tropinone, and k_{cat} values were 17.1 ± 2.5 μM, 94.9 ± 4.8 μM, and 1.19 ± 0.02 s^{-1}, respectively (see below). Judged by these results, substrate concentrations of the flowing solution and its flow rates in this study were high enough to ensure the saturation of the enzyme molecules in the crystal with the substrates and to achieve the steady state (*7*). Also, the modest catalytic rate allows substrate diffusion and binding events to successfully compete with enzyme catalysis, enabling the accumulation of the enzyme−substrate complex in the crystal.

Data Processing and Structure Determination. The diffraction data were processed with the Daresbury Laue suite of programs (*8*) with some in-house modifications by T. Higashi. It is worth noting that the energy deconvolution was performed based on Ren and Moffat's algorithm (*9*), resulting in the uniform distribution of the completeness over the resolution bins (Table 1). Structure refinement was carried out with X-PLOR 3.851 (*10*) using the atomic coordinates of the TR-II−$NADP^+$−ψ-tropine complex (PDB code: 2ae2) (*5*). The parameter and topology files for NADPH and

tropinone were generated with XPLO2D (*11*). Refinement included rigid body, positional, and individual B-factor steps, followed by manual rebuilding with TURBO-FRODO (*12*). Crystallographic occupancy estimation for the bound substrates was carried out with a grouped, unrestrained occupancy refinement protocol in CNS (*13*) with settings of each substrate molecule as a group, the occupancy value for the other part at 1.0, and B-factor values fixed at the final refined values. The estimated occupancy values were not included in the refinement process or the final models, and 1.0 was used instead.

Single-Crystal Spectrophotometry. Microspectrophotometric measurement was carried out on a single TR-II crystal using PMA50 system (Hamamatsu Photonics, Japan) with a Xe lamp and mirror objective lenses at room temperature. Spectra were collected using a 0.05 mm diameter light beam and exposure times of 1 s with 100× integration per spectrum. Absorption spectra of (i) the TR-II−NADPH crystal, (ii) the TR-II−NADPH−tropinone crystal with flow, and (iii) the TR-II−NADPH−tropinone crystal without flow were measured with (a) the TR-II−NADPH crystal with a 0.1 mL/min flow of a solution containing 4 mM NADPH, (b) the same crystal with a 1.0 mL/min flow of a solution containing 4 mM NADPH and 110 mM tropinone, 15 min after initiating the flow, and (c) the same crystal 15 min after stopping the flow, respectively. Compositions of the solutions and the other experimental conditions were the same as those at the data collection. A reference spectrum was recorded at the same position of the crystal after completion of the reaction and substitution with a solution containing 4 mM $NADP^+$ without tropinone.

NADPH concentration was calculated from the difference absorbance at $A_{340\ nm} - A_{430\ nm}$. The millimolar concentration of the TR-II−NADPH−tropinone complex, *c*, in the crystal with the flow was evaluated from the following equation:

$$[\{\text{NADPH concentration in (i) (17.3 mM)} + 4\ \text{mM} \times \text{solvent content in (i) (0.689)}\} \times d + 4\ \text{mM} \times (0.7\ \text{mm} - d)]/[\{c + 4\ \text{mM} \times \text{solvent content in (ii) (0.688)}\} \times d + 4\ \text{mM} \times (0.7\ \text{mm} - d)] = \text{Abs(i)/Abs(ii)}$$

by assuming the TR-II−NADPH crystal (condition i) has 100% occupancy of NADPH, the concentration of NADPH of the solution inside and around the crystal was 4 mM, the diameter of the capillary was 0.7 mm, and the crystal thickness, *d*, was 0.2−0.4 mm, as usually observed values. The occupancy of the TR-II−NADPH−tropinone complex in the crystal with flow (condition ii) was calculated using an enzyme concentration in the crystal of 17.4 mM. The occupancy of the TR-II−NADPH−tropinone complex in the crystal without the flow (condition iii) was estimated from the ratio of Abs(iii)/Abs(i), by assuming the crystal settled to equilibrium and the NADPH/$NADP^+$ ratios in the crystal and the surrounding solution were the same.

Enzyme Assay and Kinetic Analysis. TR-II enzymatic activity was measured spectrophotometrically by monitoring NADPH oxidation at 340 nm using a molar absorption coefficient of 6200 M^{-1} cm^{-1} for NADPH. Reactions were performed in 0.1 M HEPES-Na, pH 7.5, 2.0 M Li_2SO_4, and 1 mM DTT at 15 °C. The apparent K_m values for NADPH and tropinone were determined by monitoring the enzyme activity with various concentrations of NADPH or tropinone at a fixed saturating concentration of tropinone (4 mM) or NADPH (0.2 mM), respectively. The protein concentration was determined according to Bradford (*14*) using bovine serum albumin as a standard. Kinetic constants were determined by direct fitting to the Michaelis−Menten equation with the Marquardt method.

RESULTS AND DISCUSSION

Data Collection Strategy. The rate of the forward reaction of TR-II is much faster than that of the reverse reaction (*2*, *15*) (Scheme 1). To capture the structure of the TR-II enzyme−substrate complex prior to the reaction proceeding, we adopted two strategies in the X-ray experiment: continuous supply of the substrates to the crystal and fast data collection. Continuous supply of the substrates to the crystal was required to secure binding of both substrates to the enzyme, and this was accomplished by the continuous flow of NADPH and tropinone through the flow-cell at a fast flow rate. The remarkably large solvent content (c.a. 69%) and small intermolecular contacts around the active site in the crystal used in this study probably allow smooth substrate diffusion and exchange in the crystal. In addition, we used a slightly shifted reaction pH (pH 7.5) from the optimal pH (around pH 5.3−6.5 (*2*, *15*)) to retard the catalytic rate of the enzyme and thus to enable the accumulation of the TR-II enzyme−substrate complex in the crystal. The data measured from the crystal using a further shifted reaction pH as pH 10.0, however, gave no clear electron density for tropinone at the active site (data not shown). The flow-cell method is also useful to collect several data sets from one crystal under different conditions by changing the composition of flowing solution. Thus, we collected two data sets from the same crystal in two distinct states, one in the complex with NADPH and the other complexed with both NADPH and tropinone, which was realized by introducing tropinone within the same crystal. Such an experiment made it possible to depict the structural differences of the enzyme with or without tropinone, under otherwise identical conditions.

The best strategy for attaining fast and high-resolution data collection under the current experimental conditions is considered to be a Laue experiment with a highly brilliant white X-ray beam from a synchrotron and a large detector area, for the following reasons: (1) As the crystal has a large unit cell, a large area detector such as a large imaging plate (IP) is necessary, and a relatively small area CCD detector is not appropriate. (2) The crystals should not be frozen during synchrotron data collection for the flow-cell experiment, thus requiring quick data collection to avoid radiation damage on the crystal. A conventional monochromatic data collection with IP, however, needs a certain amount of time. (3) The fast flow rate we employed on the flow-cell experiment sometimes causes a positional shift or movement of the crystal during data collection. A short exposure Laue experiment overcomes this problem. (4) Attempts on freeze-trapping of the TR-II enzyme−substrate complex that the reaction was initiated by soaking the substrate in the crystal were unsuccessful and only yielded distorted diffraction spots, indicating the high heterogeneity of the molecular species in the crystal under nonsteady-state conditions (data

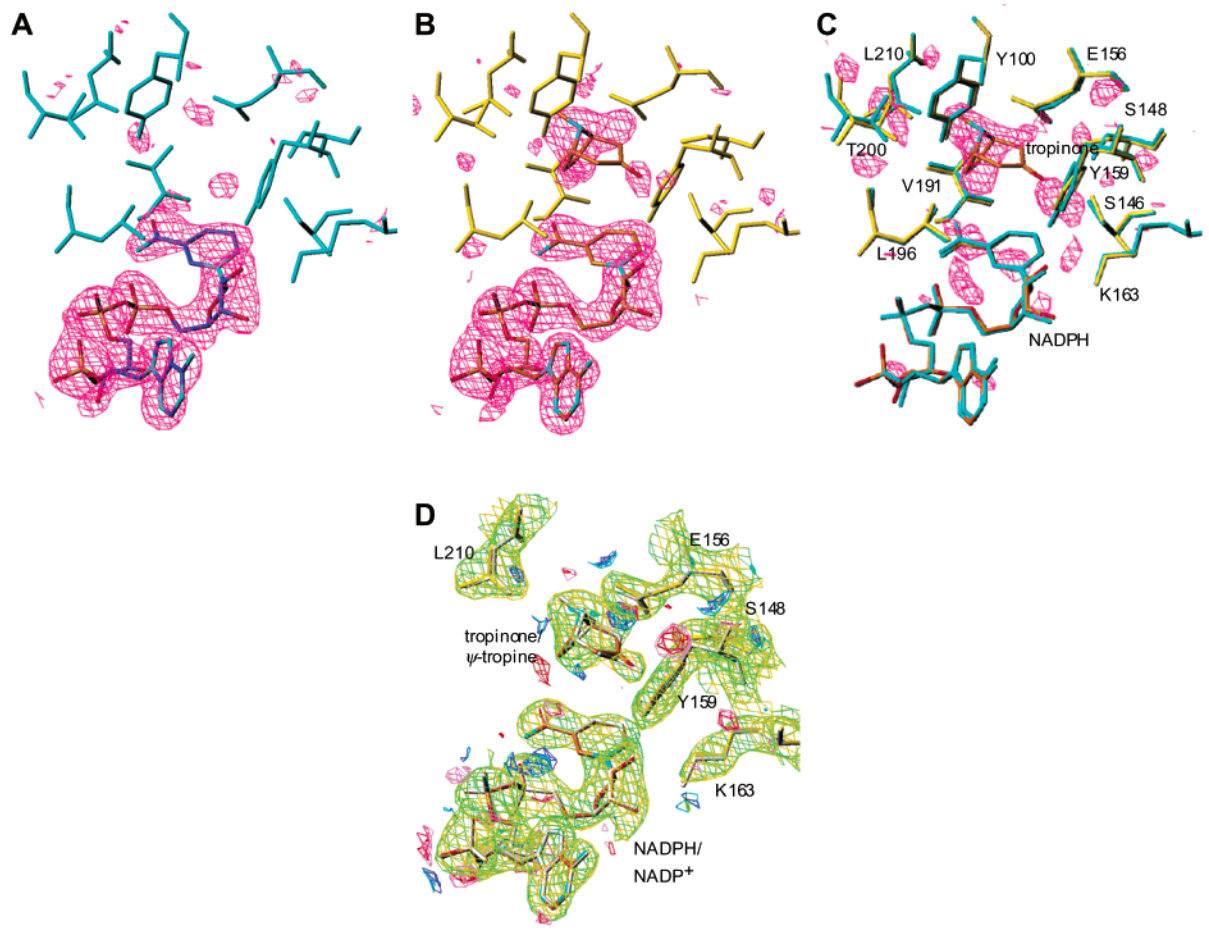

FIGURE 1: Difference electron density maps (contoured at 2.5 σ) around the TR-II active site. (A) The σA-weighted $F_o - F_c$ simulated annealing (SA)-omit map and the refined structure of the TR-II−NADPH complex (the first data series). The final refined model (omitting NADPH and water molecules) was subjected to simulated annealing run (1000 K), and the electron density map was calculated from the resultant structure. (B) The σA-weighted $F_o - F_c$ SA-omit map and the refined structure of the TR-II−NADPH-tropinone complex (the second data series). The final refined model omitting NADPH, tropinone, and water molecules was used for SA-omit map calculation in a similar manner as described in panel A. (C) The σA-weighted $[F_o$(TR-II−NADPH−tropinone) $- F_o$(TR-II−NADPH)$]\alpha_{calc}$ difference electron density map with superposed structures of the TR-II−NADPH and TR-II−NADPH−tropinone complexes shown in cyan and yellow, respectively. The phase for the map was back-calculated using the same model as used in panel A. Coordinates were superposed with LSQKAB (*23*). (D) The σA-weighted $2F_o - F_c$ maps (contoured at 1.5 σ) and the $F_o - F_c$ maps (contoured at 2.5 σ) of the second data series. The $2F_o - F_c$, positive $F_o - F_c$, and negative $F_o - F_c$ maps calculated with the final refined model of the TR-II−NADPH−tropinone complex are shown in green, blue, and red, while those calculated with the product complex model (TR-II−$NADP^+$−ψ-tropine complex; see Table 2 footnote) are show in yellow, cyan, and pink, respectively. The structures of the finally refined TR-II−NADPH−tropinone complex model and the product complex model are shown in yellow and white, respectively. The figures were generated with TURBO-FRODO (*12*).

not shown). Therefore, we collected the Laue diffraction data at BL18B, Photon Factory, using 40 × 80 cm IP. This enabled us to collect two full data sets from one crystal before the crystal was damaged. Since the TR-II crystal gives rise to streak-free Laue spots, indicating low mosaicity, this crystal is ideally suited for Laue techniques despite its large unit cell size. Data collection statistics are presented in Table 1, together with model refinement statistics. The resultant electron density maps were also of good quality, as compared to maps from monochromatic data with the same resolution limit. Although in this paper a typical data set from a single crystal is reported, the results were reproducible with two other data sets.

Michaelis Complex Structure Captured. The $F_o - F_c$ omit map of the second data series (TR-II−NADPH−tropinone complex) clearly showed the electron density of both NADPH and tropinone, while the $F_o - F_c$ omit map from the first data series (TR-II−NADPH complex) showed only the electron density of NADPH (Figure 1A,B). These results indicate that both NADPH and tropinone bound to the enzyme during the second data collection series and that the Michaelis complex formed in the flow cell. The substrate binding was further supported by the F_o(TR-II−NADPH−tropinone) $- F_o$(TR-II−NADPH) difference electron density map, showing the electron density corresponding to tropinone (Figure 1C). The occupancies for the bound substrates in both data sets were considered to be nearly 100%. This was judged by the occupancy refinement with CNS, which derived the value as in the range of 1.00−1.10 with a similar degree of B-factors as that of the protein part (Table 2), and by the electron density, which showed a similar magnitude as that of the surrounding protein models without significant residual density (Figure 1D).

To confirm that the obtained structure corresponds to the enzyme−substrate complex ES1S2, the reaction states of the TR-II crystal were monitored separately with a UV−vis microspectrophotometer under conditions identical to those of the data collection (Figure 2). The absorbance at 340 nm

Table 2: Summary of the Average B-Factors and Occupancies of the Model

		NADPH or $NADP^+$		tropinone or ψ-tropine		Tyr159[a]		protein water	
		B ($Å^2$)	occ.[b]	B ($Å^2$)	occ.[b]	B ($Å^2$)	occ.[b]	B ($Å^2$)	B ($Å^2$)
first data	A chain	11.4	1.04			7.2	1.14	14.7	22.2[c]
(TR-II−NADPH)	B chain	16.8	1.02			9.0	1.04	15.3	
second data	A chain	11.4	1.00	23.5	1.10	10.1	1.06	14.3	23.8[c]
(TR-II−NADPH−tropinone)	B chain	16.2	1.03	37.6	1.05	8.1	1.02	14.4	
second data, product model[d]	A chain	12.7	1.02	22.4	1.11	10.4	1.07	13.8	22.4[c]
(TR-II−$NADP^+$−ψ-tropine)	B chain	15.0	1.03	32.0	1.08	7.1	1.01	13.8	
monochromatic data[e]	A chain	13.1	1.02	24.4	1.04	12.4	1.06	17.9	32.3[c]
(TR-II−$NADP^+$−ψ-tropine)	B chain	19.8	0.98	35.8	1.05	13.5	1.06	18.6	

[a] For reference, the average B-factor and the occupancy values of the catalytic residue Tyr159 were estimated with the same manner and indicated. [b] The occupancy values estimated as described in Experimental Procedures. [c] The B-factor values for water indicate the average values of over all water molecules in the asymmetric unit. [d] The protein model from the second data and the product models ($NADP^+$ and ψ-tropine), instead of the substrate models (NADPH and tropinone), were subjected to the simulated annealing (at 1000 K), positional, and B-factor refinements. The *R*-factor of the resultant model is 0.197 (R_{free} = 0.273). [e] PDB code 2ae2 (*5*).

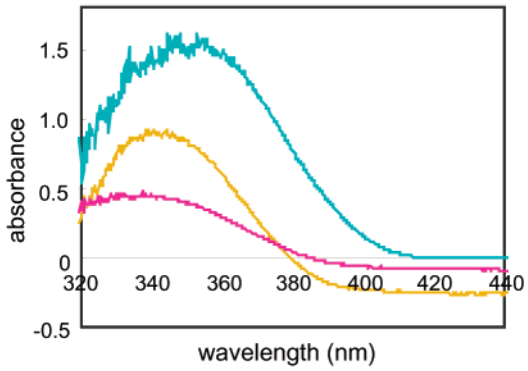

FIGURE 2: Spectroscopic analysis of the single TR-II crystal under the same experimental conditions used for the data collection. Absorption spectra of the TR-II−NADPH crystal, the TR-II−NADPH−tropinone crystal with flow, and the TR-II−NADPH−tropinone crystal without flow are shown in cyan, yellow, and pink, respectively.

somewhat changed with the introduction of tropinone to the TR-II−NADPH crystal, showing a decrease of the NADPH content in the system accompanying the catalytic reaction. The occupancy of the TR-II−NADPH−tropinone complex in the crystal under the continuous flow of the substrates solution was estimated to be in the range of about 60−70%. This indicates that the majority of the enzyme molecules in the crystal are trapped as an enzyme−substrate complex under the experimental condition of the second data series. Thus, the obtained structure could be regarded as ES_1S_2, although the reaction proceeded to some extent. When the supply of substrates was stopped, the absorbance greatly diminished, and the estimated occupancy of ES_1S_2 decreased to about 35%. The results were reproducible with two other measurements using independent crystals (data not shown).

On the basis of this result, the enzyme−substrate complex (TR-II−NADPH−tropinone) was finally modeled and refined against the second data (Tables 1 and 2). Even if the enzyme−product complex (TR-II−$NADP^+$−ψ-tropine) was modeled and subjected to the refinement against the second data, the positions and orientations of the ligands and residues in the resultant model were almost the same as those of the substrate complex model (Figure 1D), reflecting the fact that the substrates and the products only differ in one hydrogen at C4-carbon in the nicotinamide ring of NADPH and $NADP^+$, or two hydrogen atoms at the C3-carbonyl group of tropinone and ψ-tropine. The product complex model also gave the similar statistics and electron density maps as the substrate complex model (Table 2 and Figure 1D).[2]

Rotational Movement of the Substrate. The structure of the TR-II−NADPH−tropinone complex enabled us to compare the structures of ES_1S_2 and EP_1P_2. The TR-II−NADPH−tropinone complex (ES_1S_2) exhibits small but significant structural differences at the active site, as compared with that of the TR-II−$NADP^+$−ψ-tropine complex (EP_1P_2) reported previously (*5*) (Figure 3). The F_o-(ES_1S_2) − F_o(EP_1P_2) difference electron density map showed several peaks around the binding substrate: one is a minus peak at the hydroxyl group and the methylene bridge of ψ-tropine, and the others are plus peaks above the methylene bridge and below the methyl group. These peaks indicate that the substrate molecule slightly changes its binding orientation before and after the catalytic process. That is, before the catalytic reaction, the carbonyl and the methylene groups of tropinone are likely to be moved further from the cofactor, whereas the methyl group is moved closer to the cofactor, as compared with the product (ψ-tropine) within the crystal. This is a seesaw-like rotational movement (Figure 3). Similar peaks of the difference electron density around the binding substrate were also found in another molecule in an asymmetric unit, in the two other independent experiments as described above, and in other difference maps calculated with phases derived from the other models, including the protein models of the TR-II−NADPH−tropinone complex (ES_1S_2) structure and of the TR-II−$NADP^+$−ψ-tropine complex (EP_1P_2) structure but not observed in maps calculated using the first data series in this study or the data measured at pH 10.0 (see Supporting Information).

Implication for Catalysis. The movement of the substrate described above is favorable for the geometry required for the catalytic reaction mechanism of TR-II. The reaction requires the proton transfer to the carbonyl group of tropinone from the catalytic residue Tyr159 Oη, and the nucleophilic attack of the pro-S hydride of NADPH on the carbonyl carbon of tropinone. On the other hand, because the products are simply the substrates for the reverse reaction, the EP_1P_2

[2] Please note that all the $F_o - F_o$ difference maps in this study (Figure 1A−C and Figure 3) were calculated with the phases from the simulated annealing (SA)-omit protein model, neither including the substrates nor the products, so that they are free from the biases derived from the interpretation of the ligands whether they are the substrates or the products.

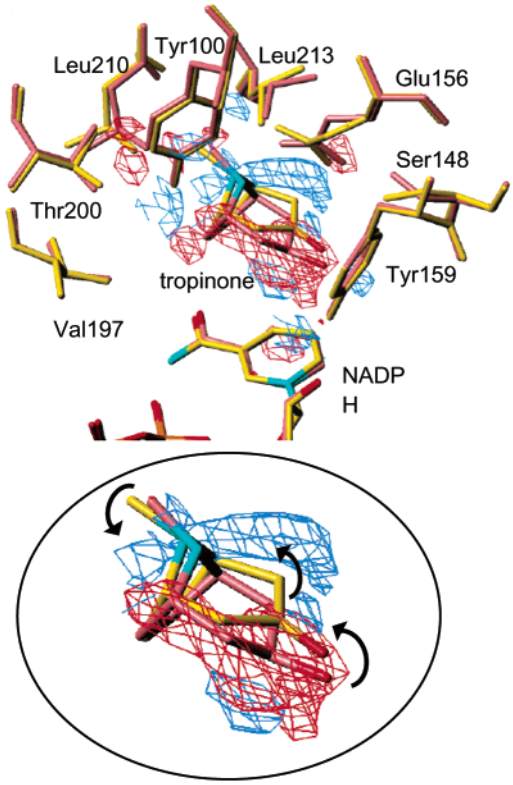

FIGURE 3: Active site structures of the TR-II−NADPH−tropinone complex (the ES_1S_2 complex) and the TR-II−$NADP^+$−ψ-tropine complex (the EP_1P_2 complex (*5*)) with the σA-weighted difference map [$F_o(ES_1S_2) - F_o(EP_1P_2)$] α_{calc} (contoured at 2.5 σ). The phase for the map was back-calculated in a similar manner as described in Figure 1B. Blue contours depict electron density that appears in the ES_1S_2 complex; red contours depict diminished electron density. Residues of the ES_1S_2 complex and the EP_1P_2 complex are shown in yellow and pink, respectively. Coordinates were superposed with LSQKAB. Magnification of the tropinone binding region is shown in the circled region. The figure was generated with TURBO-FRODO.

state can be regarded as an enzyme−substrate complex for the reverse reaction. The reverse reaction implies the proton transfer from ψ-tropine to Tyr159 and the nucleophilic attack of a hydride on $NADP^+$. The attack angles in model hydride transfer reactions and in dehydrogenase reactions have been suggested to be obtuse angles (*16*−*21*). In the EP_1P_2 complex, the observed arrangement of ψ-tropine, $NADP^+$, and Tyr159 was appropriate for the hydride attack on the $NADP^+$ nicotinamide ring (*5*) (Figure 4A). If this arrangement were strictly kept in the ES_1S_2 complex, then the attack angle of the pro-S hydride of NADPH on the carbonyl carbon of tropinone would be an acute angle (Figure 4B). To make the attack angle obtuse, NADPH, or tropinone, or both should rotate relative to the enzyme. In the ES_1S_2 complex elucidated in this study, the tropinone molecule exhibits a seesaw-like rotation and significantly changes its orientation relative to the enzyme to assume the favorable geometry for the hydride attack (Figure 4C). Thus, on the side of NADPH, the nicotinamide group alone exhibited only a subtle shift to readjust the reaction geometry to tropinone (Figure 3). In the refined models of tropinone, the rotation must be underestimated so that the actual orientation of tropinone in the ES_1S_2 state could be further rotated relative to the refined model. This is because the crystal used in this study probably contained a mixture of two populations, ES_1S_2 and EP_1P_2 complexes, as judged by the spectroscopic analysis described above. The alignments in the TR-II active sites agree well with the concept of the near attack conformer (*22*), defined as the required conformation for juxtaposed reactants to enter a transition state. This conformer associated with the Michaelis complex is considered to make important contributions to the rates of enzymatic reactions.

Comparison of the Active Sites of the ES_1S_2 and EP_1P_2 Structures. The active sites in both the ES_1S_2 and the EP_1P_2 complexes showed a high degree of complementarity for binding tropinone or ψ-tropine (Figure 5A,B). The residues exhibit small but significant shifts for this complementarity. For example, in the ES_1S_2 complex, Glu156 moved as if to push down the amine group of tropinone; Ser148 moved as if to assist the Glu156 movement; and Thr 200, Leu210, and Leu213 swung away to avoid a steric crush with the methyl group (Figure 3). The side chain of Tyr159 also changed its position slightly. These residue movements are in accordance with the difference in the binding modes between tropinone and ψ-tropine, suggested from the F_o-$(ES_1S_2) - F_o(EP_1P_2)$ difference electron density map. Besides them, no large conformational change was observed between the ES_1S_2 and the EP_1P_2 complexes. The two structures are superposed with a Cα root-mean-square deviation (rmsd) of 0.19 Å. The positional shifts of the active site residues mentioned above would occur within a range of the same framework.

Step-by-Step Visualization of the Catalytic Reaction. The two structures elucidated in this study, the TR-II−NADPH

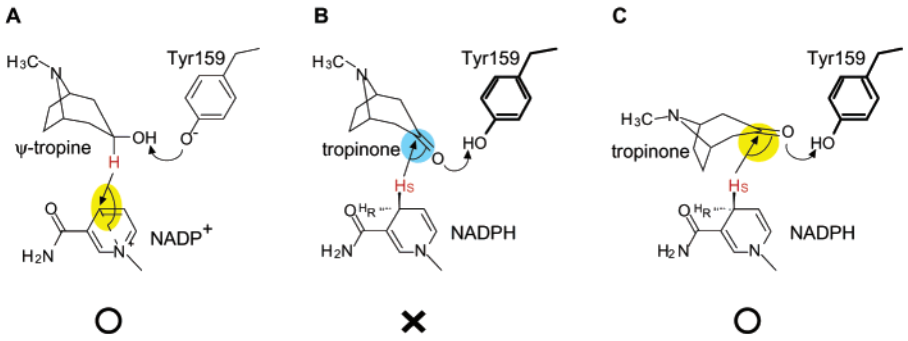

FIGURE 4: Schematic drawings of the reaction geometry of the substrate, the cofactor, and the catalytic residue (Tyr159) in TR-II ternary complexes. (A) The TR-II−$NADP^+$−ψ-tropine complex (EP_1P_2). The hydride attack angle (highlighted in yellow) was observed as an obtuse angle (*5*). (B) The TR-II−NADPH−tropinone complex (ES_1S_2) with the same catalytic geometry as that of the EP_1P_2 complex. The hydride attack angle (highlighted in blue) would be acute. (C) The TR-II−NADPH−tropinone complex (ES_1S_2) with the geometry observed in this study. The hydride attack angle (highlighted in yellow) would be obtuse.

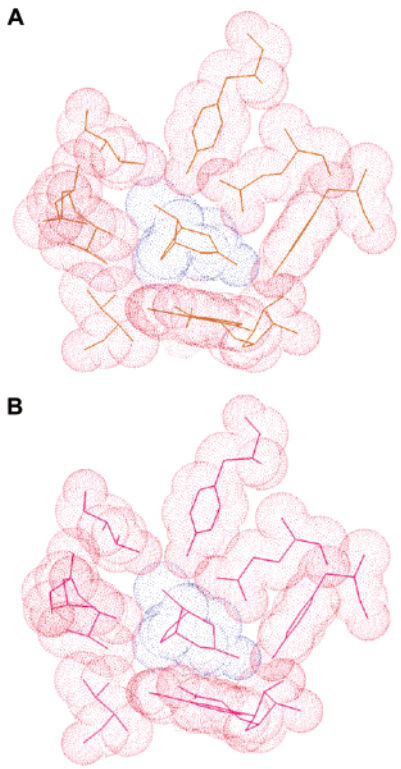

FIGURE 5: Dotted van der Waals surfaces of the active site cavity in the TR-II−NADPH−tropinone complex (the ES_1S_2 complex) and the TR-II−$NADP^+$−ψ-tropine complex (the EP_1P_2 complex (*5*)). (A) The TR-II ES_1S_2 complex. Surfaces of the active site and tropinone are shown in red and indigo, respectively. (B) The TR-II EP_1P_2 complex. Color settings are the same as in panel A. The figures were generated with TURBO-FRODO.

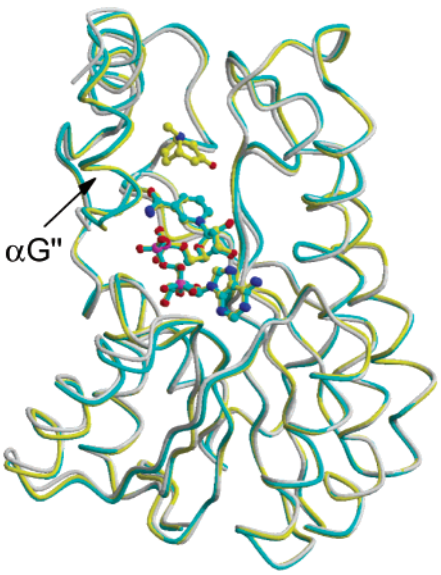

FIGURE 6: Superposition of the subunit structures of the TR-II−NADPH and TR-II−NADPH−tropinone complexes with the structure of unliganded TR-II (*4*). Coordinates were superposed with LSQKAB. The Cα backbones of TR-II−NADPH, TR-II−NADPH−tropinone, and the unliganded TR-II are shown in cyan, yellow, and gray, respectively. Bound NADPH and tropinone are illustrated in ball-and-stick models. The position of αG″ is shown with an arrow. The figure was generated with MOLSCRIPT (*24*) and Raster3D (*25*).

and TR-II−NADPH−tropinone complexes, together with the TR-II unliganded structure (*4*) (Figure 6) enabled us to follow the reaction pathway between the E and the ES1S2 steps in detail, as the reaction is likely to proceed by an ordered sequential mechanism, with the cofactor (NADPH; S1) binding first. First, the electron density of the helix αG″, which is disordered in the TR-II E state structure (*4*), was clearly observed even in the TR-II−NADPH complex (ES1), as well as in the TR-II−NADPH−tropinone complex (ES1S2) (Figure 6). Some residues important for the cofactor and substrate binding are located in αG″ (5). The backbone of the active site in TR-II is arranged almost properly even when the cofactor (S1) is solely bound to the active site. Next, a comparison of the refined structures between the TR-II−NADPH (ES1) and TR-II−NADPH−tropinone (ES1S2) complexes revealed small conformational changes at the side chains of some residues, such as Ser146, Ser148, Tyr159, Val191, Leu196, Thr200, and Leu210 (Figure 1C). These are the residues interacting with the cofactor and/or the substrate, as observed in this study and previously (5). When the substrate (tropinone; S2) binds to the active site, these residues probably rearrange their postures and provide complementarity to the binding substrate, as mentioned above. No large main-chain conformational changes were observed between the TR-II−NADPH and the TR-II−NADPH−tropinone complexes (Cα rmsd 0.23 Å).

CONCLUSIONS

The results obtained in this study indicate that the participants of an enzymatic reaction (the substrate, the cofactor, and the catalytic residue(s)) are considered to assume the most appropriate geometry so as to allow the reaction to proceed at that point of the reaction. The side chains at the active sites of an enzyme are likely to adjust the substrate orientation favorable for the reaction. An enzyme should provide properly aligned reaction geometries that are favorable for each reaction step.

ACKNOWLEDGMENT

We gratefully acknowledge Drs. N. Watanabe, M. Suzuki, N. Igarashi, and N. Sakabe for help with data collection at BL-18B, Photon Factory; Y. Kawano for help with single crystal microspectrophotometry; K. Nakajima and T. Hashimoto for providing the TR-II expression system and various discussions; K. Sakata for support for computational work; and Y. Maéda for continuous support, encouragement, and critical reading of the manuscript. The refinement program was run on a computer at the Supercomputer Laboratory, Institute for Chemical Research, Kyoto University.

SUPPORTING INFORMATION AVAILABLE

Electron density maps at a protein region together with statistics of diffraction data completeness and difference electron density maps at the active site calculated under various conditions. This material is available free of charge via the Internet at http://pubs.acs.org.

REFERENCES

1. Petsko, G. A., and Ringe, D. (2000) *Curr. Opin. Chem. Biol. 4*, 89−94.
2. Hashimoto, T., Nakajima, K., Ongena, G., and Yamada, Y. (1992) *Plant Physiol. 100*, 836−845.
3. Nakajima, K., Hashimoto, T., and Yamada, Y. (1993) *Proc. Natl. Acad. Sci. U.S.A. 90*, 9591−9595.

4. Nakajima, K., Yamashita, A., Akama, Y., Nakatsu, T., Kato, H., Hashimoto, T., Oda, J., and Yamada, Y. (1998) *Proc. Natl. Acad. Sci. U.S.A. 95*, 4876−4881.
5. Yamashita, A., Kato, H., Wakatsuki, S., Tomizaki, T., Nakatsu, T., Nakajima, K., Hashimoto, T., Yamada, Y., and Oda, J. (1999) *Biochemistry 38*, 7630−7637.
6. Yamashita, A., Nakajima, K., Kato, H., Hashimoto, T., Yamada, Y., and Oda, J. (1998) *Acta Crystallogr. D54*, 1405−1407.
7. Stoddard, B. L., and Farber, G. K. (1995) *Structure 3*, 991−996.
8. Helliwell, J. R., Habash, J., Cruickshank, D. W. J., Harding, M. M., Greenhough, T. J., Campbell, J. W., Clifton, I. J., Elder, M., Machin, P. A., Papiz, M. Z., and Zurek, S. (1989) *J. Appl. Cryst. 22*, 483−497.
9. Ren, Z., and Moffat, K. (1995) *J. Appl. Cryst. 28*, 482−493.
10. Brünger, A. T. (1992) *X-PLOR Manual Version 3.1.*, Yale University Press, New Haven, CT.
11. Kleywegt, G. J., and Jones, T. A. (1997) *Methods Enzymol. 277*, 208−230.
12. Roussel, A., and Cambillau, C. (1996) *TURBO-FRODO Mannual*, AFMB-CNRS, Marseille, France.
13. Brünger, A. T., Adams, P. D., Clore, G. M., DeLano, W. L., Gros, P., Grosse-Kunstleve, R. W., Jiang, J.-S., Kuszewski, J., Nilges, M., Pannu, N. S., Read, R. J., Rice, L. M., Simonson, T., and Warren, G. L. (1998) *Acta Crystallogr. D54*, 905−921.
14. Bradford, M. M. (1976) *Anal. Biochem. 72*, 248−254.
15. Portsteffen, A., Dräger, B., and Nahrstedt, A. (1994) *Phytochemistry 37*, 391−400.
16. Liberles, A. (1968) *Theoletical organic chemistry*, The MacMillan Co., Toronto, Ontario.
17. Burgi, H. B., Lehn, J. M., and Wipff, G. (1974) *J. Am. Chem. Soc. 96*, 1956−1957.
18. Houk, K. N., Paddon-Row, M. N., Rondan, N. G., Wu, Y. D., Brown, F. K., Spellmeyer, D. C., Metz, J. T., Li, Y., and Loncharich, R. J. (1986) *Science 231*, 1108−1117.
19. Wu, Y. D., and Houk, K. N. (1987) *J. Am. Chem. Soc. 109*, 2226−2227.
20. Wu, Y. D., and Houk, K. N. (1987) *J. Am. Chem. Soc. 109*, 906−908, 908−910.
21. Sherrod, M. J., and Menger, F. M. (1989) *J. Am. Chem. Soc. 111*, 2611−2613.
22. Bruice, T. C., and Benkovic, S. J. (2000) *Biochemistry 39*, 6267−6274.
23. Collaborative Computational Project, No. 4 (1994) *Acta Crystallogr. D50*, 760−763.
24. Kraulis, P. J. (1991) *J. Appl. Cryst. 24*, 946−950.
25. Meritt, E. A., and Murphy, M. E. P. (1994) *Acta Crystallogr. D50*, 869−873.

BI0272712